Fission-like events in the $^{12}C + ^{169}Tm$ system at low excitation energies

Arshiya Sood,[1,*] Pushpendra P. Singh,[1,†] Rudra N. Sahoo,[1] Pawan Kumar,[1] Abhishek Yadav,[2] Vijay R. Sharma,[2] Mohd. Shuaib,[7] Manoj K. Sharma,[3] Devendra P. Singh,[4] Unnati Gupta,[5] R. Kumar,[2] S. Aydin,[6] B. P. Singh,[7] H. J. Wollersheim,[1,8] and R. Prasad[7]

[1]*Department of Physics, Indian Institute of Technology Ropar, Rupnagar 140 001, Punjab, India*
[2]*Inter-University Accelerator Center, New Delhi 110 067, India*
[3]*Department of Physics, S. V. College, Aligarh 202 001, Uttar Pradesh, India*
[4]*Department of Physics, University of Petroleum and Energy Studies, Dehradun 248 007, Uttarakhand, India*
[5]*Department of Physics, Delhi University, New Delhi 110 067, India*
[6]*Department of Physics, University of Aksaray, Aksaray, Turkey*
[7]*Department of Physics, A. M. University, Aligarh 202 002, Uttar Pradesh, India*
[8]*GSI Helmholtzzentrum für Schwerionenforschung, Planckstrasse 1, 64291 Darmstadt, Germany*

(Received 26 May 2017; published 28 July 2017)

Background: Fission has been found to be a dominating mode of deexcitation in heavy-ion induced reactions at high excitation energies. The phenomenon of heavy-ion induced fission has been extensively investigated with highly fissile actinide nuclei, yet there is a dearth of comprehensive understanding of underlying dynamics, particularly in the below actinide region and at low excitation energies.
Purpose: Prime objective of this work is to study different aspects of heavy-ion induced fission ensuing from the evolution of composite system formed via complete and/or incomplete fusion in the $^{12}C + ^{169}Tm$ system at low incident energies, i.e., $E_{lab} \approx 6.4$, 6.9, and 7.4 A MeV, as well as to understand charge and mass distributions of fission fragments.
Method: The recoil-catcher activation technique followed by offline γ spectroscopy was used to measure production cross sections of fission-like events. The evaporation residues were identified by their characteristic γ rays and vetted by the decay-curve analysis. Charge and mass distributions of fission-like events were studied to obtain dispersion parameters of fission fragments.
Results: In the present work, 26 fission-like events ($32 \leqslant Z \leqslant 49$) were identified at different excitation energies. The mass distribution of fission fragments is found to be broad and symmetric, manifesting their production via compound nuclear processes. The dispersion parameters of fission fragments obtained from the analysis of mass and isotopic yield distributions are found to be in good accord with the reported values obtained for different fissioning systems. A self-consistent approach was employed to determine the isobaric yield distribution.
Conclusions: The present work suggests that fission is one of the competing modes of deexcitation of complete and/or incomplete fusion composites at low excitation energies, i.e., $E^* \approx 57$, 63, and 69 MeV, where evaporation of light nuclear particle(s) and/or γ rays are assumed to be the sole contributors. A single peaked broad Gaussian mass dispersion curve has corroborated the absence of any noncompound nuclear fission at the studied energies.

DOI: 10.1103/PhysRevC.96.014620

I. INTRODUCTION

Since the discovery of nuclear fission [1], it has inspired a great deal of effort across the globe and has been prodigiously investigated in light- and heavy-ion induced reactions on actinide targets [2]. The cross-section data for fission fragments in a diverse range of projectile-target combinations are essential for applications in the areas of superheavy element synthesis, nuclear astrophysics, nuclear energy, and radiochemistry for national security. They are also of fundamental importance for the development of next generation nuclear reactors for the production of nuclear energy and transmutation of commercial nuclear waste [3,4]. The accurate knowledge of fission dynamics and cross-sections is required to optimize the production of new heavy radioactive isotopes of interest. Fission plays a vital role in ascertaining the stability of superheavy nuclei [5]. In macroscopic theories of heavy-ion collisions, the energy of the colliding nuclei is the sum of repulsive electrostatic energy and attractive nuclear energy. Moller and Sierk [6] suggested that the multidimensional potential "energy landscape" sways the dynamics of the fusion process from the touching configuration of two nuclei to the formation of a compound system, equilibrated in all degrees of freedom. The topography of the potential energy landscape is, however, different for the fusion of lighter and heavier systems because for the latter the electric forces are relatively stronger. Additionally, the inclusion of microscopic effects, which arise because neutrons and protons inside the nuclei obey quantum mechanical laws, is of paramount importance for the theoretical studies of nuclear collisions. The other factors—, deformation of colliding nuclei, their mass-asymmetry, separation between the two, and the nature of neck joining them, together with the microscopic effects—increases the complexity in theoretical reckoning of the path taken by the system through its evolution. Consequently, different experimental probes have been used to explicate the path

*arshiya.sood@iitrpr.ac.in
†pps@iitrpr.ac.in

traversed by the system. Nishio *et al.* [7] and Hinde *et al.* [8], measured the angular distributions of fission fragments and the production cross sections of evaporation residues to investigate the aforementioned aspects. The conclusions of both the works are well described by macroscopic models but they have contradictory interpretations in determining the path taken by the system: the fusion meadow or the fission valley [6]. Recently, Ghosh *et al.* [9], proposed that the accurate measurement of mass distribution as a function of excitation energy can be used as a probe to determine the path followed by the system. They performed measurements for spherical and deformed targets with different projectiles, and picked up microscopic effects to determine the different topological paths a system follows through the energy landscape. It has been reported that the width of the mass distribution of fission fragments from fusion-fission reactions on a deformed target increases with the increase in excitation energy near the Coulomb barrier, whereas there is a smooth variation in the width of the mass distribution for a spherical target.

Over last few decades, heavy-ion induced reactions have captivated nuclear physicists, as they offer the most drastic rearrangement of nucleons in a many-body system [10]. In a fusion-fission process, the compound nucleus formed via complete and/or incomplete fusion may proceed towards fission depending upon the available excitation energy. Other entrance channel parameters, i.e., mass asymmetry ($\mu = \frac{M_T - M_P}{M_T + M_P}$), deformation, and Coulomb factor ($Z_1 Z_2$), have been found to influence the dynamics of fusion-fission. The final reaction products may be populated via the emission of light nuclear particles and characteristic γ rays from the fission fragments [11–16]. Nishio *et al.* [7] reported incomplete fusion-fission as one of the dominant reaction modes in addition to the complete fusion-fission at intermediate energies. The studies presented in Refs. [17–22] suggest that several reaction channels open up at intermediate projectile energies, i.e., $E/A \geqslant 8$ MeV.

Further, the survival probability of an excited compound nucleus against fission was first explained by Bohr and Wheeler using the liquid drop model [23]. It has been suggested that the dynamics of fission can be viewed as the passage of the fissioning nucleus over the fission barrier, which arises due to the competition between Coulomb and surface energies. According to the liquid drop model, no fission barrier exists for $Z \geqslant 104$; therefore, a symmetric, single-humped distribution of masses of fission fragments is most probable. Later, the observation of asymmetric mass distribution in majority of the experiments performed using actinide targets [24], and synthesis of elements beyond $Z = 104$ by Oganessian *et al.* [25] showed the inadequacy of the liquid drop model. This discrepancy was resolved by incorporating shell effects in the liquid drop model [26–29]. Strutinsky [26] proposed the shell corrections method and used averaged single particle energy as a correction term to the liquid drop model energy. It was found that the inclusion of the shell correction term increases the fission barrier height, thereby increasing the fission half-lives for heavy elements. Thus, shell effects play a crucial role in determining the stability of superheavy elements. It has also been observed that the asymmetry in the mass-distribution decreases at higher excitation energies, which makes the process of fission more symmetric. This may be attributed to gradual washing out of the shell effects at higher excitation energies of the composite system. It may be pointed out that the charge and mass distributions are two indispensable post-fission observables that have been extensively studied at intermediate energies to understand the fading of shell effects with excitation energy and the dynamics of the fission process. These observables act as a probe to identify different reaction mechanisms.

For many years now, the phenomenon of nuclear fusion-fission with heavy-ions has been extensively studied for a wide range of fissility, excitation energy, and other entrance channel parameters [17,30–33]. Although a large amount of data has been generated, complete understanding of various reaction mechanisms in general, and below the actinide region in particular, is still lacking. Therefore, the dynamics of heavy-ion interactions and the comprehensive understanding of processes ensuing from the collision of the projectile and the target nuclei are significant and need to be further investigated.

In order to explore different aspects of low energy heavy-ion induced reactions, a series of experiments was performed at the Inter-University Accelerator Center (IUAC), New Delhi. In this work, the production cross sections of fission-like events were measured in $^{12}C + ^{169}Tm$ system at projectile energies 77.18, 83.22, and 89.25 MeV. The mass and charge distributions of reaction residues likely to be populated via fission of complete and/or incomplete fusion at these energies were studied. Experimental details, data reduction methodology, and the findings of present work are discussed in Sec. II. Summary and conclusions are given in Sec. III of this paper.

II. EXPERIMENTAL DETAILS AND DATA ANALYSIS

The experiments were performed at the IUAC New Delhi using the pelletron accelerator facilities. Beams of ^{12}C (E_{lab} = 77.18, 83.22, and 89.25 MeV with beam current 25–34 nA) were bombarded on a self-supporting ^{169}Tm (abundance = 100%) target foil of thickness ≈900 $\mu g/cm^2$ prepared by rolling technique. An aluminum foil of sufficient thickness was placed behind the target foil to stop recoiling reaction products. The thickness of target and catcher foil was measured using an α-transmission method in which α particles of 5.487 MeV obtained from a standard ^{241}Am source were allowed to fall on the target and catcher foils. The energy loss suffered by α particles was used to calculate thickness of the foils. A stack of target and catcher foils was installed on an aluminum target holder with a concentric hole of 1.2 cm diameter. The target-catcher foil assembly was mounted in the General Purpose Scattering Chamber (GPSC), with the target facing the beam, and irradiated for a time span of ≈ 6–8 hours depending upon the half-lives of interest.

The γ-ray activities produced in the target-catcher foil assembly after the irradiation were counted with two pre-calibrated high-purity germanium (HPGe) detectors coupled to a computer aided measurement and control (CAMAC) based data acquisition system [34]. The calibration of detectors was done using standard (^{152}Eu and ^{60}Co) γ sources of known strengths. The measurement with the standard sources was performed before and after the offline counting of irradiated

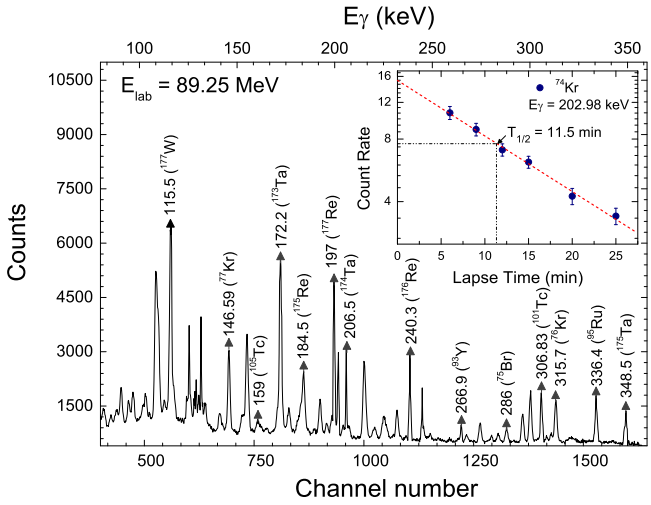

FIG. 1. A typical γ-ray spectrum of $^{12}C + ^{169}Tm$ at $E_{lab} = 89.25$ MeV. The γ lines are assigned to the different reaction products populated via complete fusion-fission and/or incomplete fusion-fission processes and evaporation residues. A typical decay curve of krypton isotope is shown in the inset. The dashed red line is the linear fit through data points.

target foils, at different detector-source separations, to vet the efficiency of the detectors. The geometry-dependent efficiency of the detectors was estimated at different detector-source separations to make efficiency corrections in the observed activities [35]. The uncertainty in the geometry dependent efficiency of the detectors was estimated to be $\leqslant 2\%$. The target-catcher stack was counted in the same geometry as that of the standard sources to circumvent the errors due to solid angle effect. The resolution of the HPGe detectors was ≈ 1.8 keV at the 1332 keV γ ray of the ^{60}Co source. Besides, the dead time of the detector was kept $\leqslant 10\%$ by adjusting the detector-stack distance for irradiated samples.

The identification of reaction products was done explicitly based on their characteristic γ rays and half-lives obtained from the decay curve analysis. A typical γ-ray spectrum obtained at $E_{lab} = 89.25$ MeV for $^{12}C + ^{169}Tm$ system is presented in Fig. 1. γ lines assigned for different fusion- and fission-like events are marked. Decay γ lines assigned to different evaporation residues were followed at increasing times after the stop of irradiation. In order to generate decay curves for individual γ lines, the count rates for γ lines were plotted as a function of lapse time. As a representative case, the decay curve of ^{74}Kr achieved by following the 202.98 keV γ line for a lapse time of ≈ 30 min is shown in inset of Fig. 1. As shown in this figure, the activity reduced to half in ≈ 11.5 min of lapse time, which is the characteristic half-life of ^{74}Kr. This confirms the identification of ^{74}Kr. Decay γ lines assigned to different evaporation residues are given in Table I along with the other spectroscopic properties [36,37]. The decay curve analysis was performed for all identified γ lines listed in this table. The intensities of the observed γ rays were used to calculate the formation cross section (σ_{ER}) of evaporation residues using the standard activation equation [35],

$$\sigma_{ER} = \frac{C_{t=0}}{N_0 \theta \phi G_\varepsilon K (1 - e^{-\lambda t_1})}, \quad (1)$$

TABLE I. Decay data of the fission fragments identified in the present work.

Serial No.	E_γ (keV)	I_γ (%)	Nuclide	Half-life ($T_{1/2}$)
1	728, 634.8	35.6, 91.2	$^{74}Br^m$	46 min
2	202.98	18	^{74}Kr	11.50 min
3	286	88	^{75}Br	96.7 min
4	264	11.4	^{75}Ge	82.78 min
5	154.6	21.1	^{75}Kr	4.29 min
6	315.7	39	^{76}Kr	14.8 h
7	146.59	37	^{77}Kr	74.4 min
8	613.8	54	^{78}As	90.7 min
9	668.1	23.4	^{79}Rb	22.9 min
10	443.3	17	^{81}Sr	22.3 min
11	881	98	^{84}Br	31.76 min
12	454	40	^{85}Zr	7.86 min
13	627.7	32.6	^{86}Y	14.74 h
14	201	96.4	^{87}Zr	1.68 h
15	947.7	10	^{89}Rb	15.15 min
16	266.9	7.4	^{93}Y	10.18 h
17	367.2	75	^{94}Ru	51.8 min
18	336.4	69.9	^{95}Ru	1.64 h
19	657.8	98.2	^{97}Nb	72.1 min
20	657.8	98.2	$^{98}Nb^m$	51.3 min
21	306.83	89	^{101}Tc	14.02 min
22	630.2	16.1	$^{102}Tc^m$	4.35 min
23	358	89	^{104}Tc	18.3 min
24	941.6	25	^{104}Ag	69.2 min
25	159	10.2	^{105}Tc	7.6 min
26	787.3	93.4	^{105}In	5.07 min

where $C_{t=0}$ is the count rate at the end of irradiation, N_0 is the initial number of target nuclei per unit area, θ is the branching ratio of the characteristic γ rays, G_ε is the geometry dependent efficiency of the detector, K is the self-absorption correction factor, λ is the decay constant of the evaporation residue, and t_1 is the duration of irradiation.

The cross sections of evaporation residues populated via fusion and/or fission-like events in $^{12}C + ^{169}Tm$ system at 77.18, 83.22, and 89.25 MeV energies are presented in Table II with experimental uncertainties. The uncertainty in the production cross sections may arise due to various factors given elsewhere [35]. The overall error in the measured cross sections is estimated to be $\leqslant 13\%$.

In order to establish the credibility of the method used to obtain measured cross sections of the fission fragments, the cross sections of evaporation residues populated via complete and/or incomplete fusion in $^{12}C + ^{169}Tm$ reaction were analyzed in the framework of the Projected Angular momentum Coupled Evaporation (PACE) [38] code, version 4.0. The code PACE4 is a statistical model code based on the Hauser-Feshbach formalism and uses the Monte Carlo method to follow the deexcitation of a compound nucleus [39,40]. It may be pointed out that the code PACE4 takes into account only a complete fusion reaction; therefore, any deviation in experimental cross-sections as compared to the theoretical model predictions may be attributed to some physical effect which is not included in the code.

TABLE II. Formation cross sections of the fission products and evaporation residues populated in the $^{12}C + ^{169}Tm$ reaction at E_{lab} = 89.25, 83.22, and 77.18 MeV.

	Cross sections σ (mb)		
Nuclide	89.25 MeV	83.22 MeV	77.18 MeV
$^{74}Br^{m}$	9.5 ± 0.8	7.6 ± 0.6	5.1 ± 0.4
^{74}Kr	4.5 ± 0.5	2.6 ± 0.3	
^{75}Br	12.1 ± 0.9	8.5 ± 0.7	6.3 ± 0.5
^{75}Ge	8.6 ± 0.9	5.3 ± 0.6	3.8 ± 0.4
^{75}Kr	14.7 ± 1.3	11.2 ± 1.3	7.2 ± 0.8
^{76}Kr	13.4 ± 1.1	13.2 ± 1.2	6.7 ± 0.7
^{77}Kr	3.1 ± 0.4	4.2 ± 0.5	
^{78}As	12.4 ± 0.9	8.4 ± 0.9	7.1 ± 0.8
^{79}Rb	17.1 ± 1.4	14.5 ± 1.6	8.9 ± 0.9
^{81}Sr	8.3 ± 0.8	8.3 ± 0.9	7.4 ± 0.7
^{84}Br	14.3 ± 1.3	11.3 ± 1.2	8.6 ± 0.9
^{85}Zr	18.6 ± 1.4	14.1 ± 1.5	11.3 ± 1.1
^{86}Y	11.6 ± 1.0	9.5 ± 0.8	9.6 ± 0.6
^{87}Zr	15.1 ± 1.5	16.5 ± 1.4	12.1 ± 1.2
^{89}Rb	13.2 ± 1.2	11.2 ± 1.0	9.4 ± 0.7
^{93}Y	15.7 ± 1.6	11.5 ± 1.3	9.3 ± 0.8
^{94}Ru	12.4 ± 1.4	9.4 ± 1.0	8.6 ± 0.6
^{95}Ru	14.9 ± 1.2	13.9 ± 1.4	9.7 ± 0.8
^{97}Nb	13.7 ± 1.5	14.3 ± 1.1	10.8 ± 0.9
$^{98}Nb^{m}$	14.6 ± 1.2	14.3 ± 1.1	7.8 ± 0.7
^{101}Tc	3.1 ± 0.3	2.9 ± 0.5	
$^{102}Tc^{m}$	12.8 ± 1.3	10.6 ± 1.4	8.7 ± 0.7
^{104}Tc	15.3 ± 1.4	12.9 ± 1.1	7.4 ± 0.6
^{104}Ag	11.6 ± 0.9	15.6 ± 1.3	7.9 ± 0.6
^{105}Tc	3.9 ± 0.5	3.5 ± 0.5	
^{105}In	9.7 ± 1.1	6.8 ± 0.7	5.2 ± 0.5
^{178}Re $(3n)$		1.6 ± 0.2	2 ± 1
^{177}Re $(4n)$	22 ± 4	90 ± 11	300 ± 24
^{176}Re $(5n)$	522 ± 73	757 ± 95	600 ± 75
^{175}Re $(6n)$	512 ± 60	180 ± 25	1.2 ± 0.3
^{177}W $(p3n)$	2.7 ± 0.6	7.6 ± 0.8	31.1 ± 4.2
^{176}Ta (αn)	93 ± 11	95 ± 11	49.4 ± 5.9
^{175}Ta $(\alpha 2n)$		0.9 ± 0.2	7.8 ± 1.4
^{174}Ta $(\alpha 3n)$	45.7 ± 6.5	64.3 ± 7.9	69.5 ± 8.3
^{173}Ta $(\alpha 4n)$	128.8 ± 18.5	70.8 ± 9.5	28.2 ± 3.6
^{171}Lu $(2\alpha 2n)$	46.1 ± 4.7	54.4 ± 5.3	37.2 ± 4.2

The experimental cross sections of $^{178,177,176,175}Re$ (xn), ^{177}W (pxn), $^{176,175,174,173}Ta$ (αxn), and ^{171}Lu $(2\alpha xn)$ residues expected to be populated via complete and/or incomplete fusion in the $^{12}C + ^{169}Tm$ system at energies E_{lab} = 77.18, 83.22, and 89.25 MeV were compared with PACE4 predictions. It was found that the xn channels are reasonably well reproduced with the theoretical calculations performed for a value of level density parameter $a = A/8$ MeV^{-1}, indicating the production of these residues via complete fusion. Therefore, the value of $a = A/8$ MeV^{-1} may be used as a default parameter for other complete fusion channels identified at this energy.

As a representative case, the ratio of experimentally measured and theoretically calculated cross sections of different residues identified at E_{lab} = 83.22 MeV is shown in Fig. 2. As shown in this figure, the ratio of experimentally measured

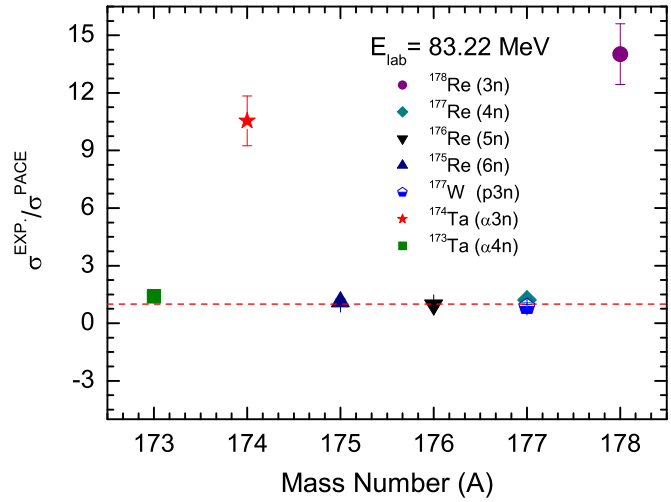

FIG. 2. Ratio of measured and PACE calculated cross sections of evaporation residues in the $^{12}C + ^{169}Tm$ reaction at E_{lab} = 83.22 MeV. Dashed lines are drawn at unity.

and theoretically calculated production cross sections of $^{177,176,175}Re$ (xn) and ^{177}W (pxn) follow the unity line, but not ^{178}Re $(3n)$. This suggests the production $^{177,176,175}Re$ and ^{177}W residues via complete fusion. However, Sharma *et al.* [41] explained the enhanced cross section in the case of ^{178}Re using the code ALICE [42]. ALICE takes into account both the equilibrium and preequilibrium components. The cross section for ^{178}Re was reasonably reproduced with the predictions of the code ALICE including rotational energy (E_{rot}) corrections. ^{178}Re was found to have contributions from both equilibrated compound nucleus decay and preequilibrium decay of three neutrons from the early stage of equilibration. Further, PACE4 underpredicts the measured cross sections of α-emitting channels. The evaporation residues $^{176,175,174,173}Ta$ are expected to be populated via both complete and/or incomplete fusion in which residues may be populated via emission of $2p3n$ from $^{181}Re^{*}$, or by fusion of one of the fragments ^{8}Be with ^{169}Tm, forming $^{177}Ta^{*}$ which may decay subsequently via one neutron. The enhanced cross sections for α-emitting channels may be a hint of the onset of incomplete fusion at this energy. The production of $^{176,175,174,173}Ta$ via $^{169}Tm(^{12}C,\alpha)^{177}Ta^{*}$ and $^{172,171}Lu$ via $^{169}Tm(^{12}C,2\alpha)^{173}Lu^{*}$ were confirmed in a recoil range distribution experiment by Chakrabarty *et al.* [43].

In the present work, the evaporation residues populated via fission were identified using the same procedure as that of complete/incomplete fusion residues presented in Fig. 2. It may be pointed out that the fission residues may originate from the deexcitation of complete/incomplete fusion composites, as the identified residues have charge and atomic mass around half the values of the residues populated via complete/incomplete fusion channels. It is pertinent to mention here that all fission residues were identified first by characteristic γ rays and then vetted by their decay-curve analysis.

A. Mass distribution of fission fragments

The mass distribution of fission fragments is an interesting post-fission probe to discern various reaction mechanisms

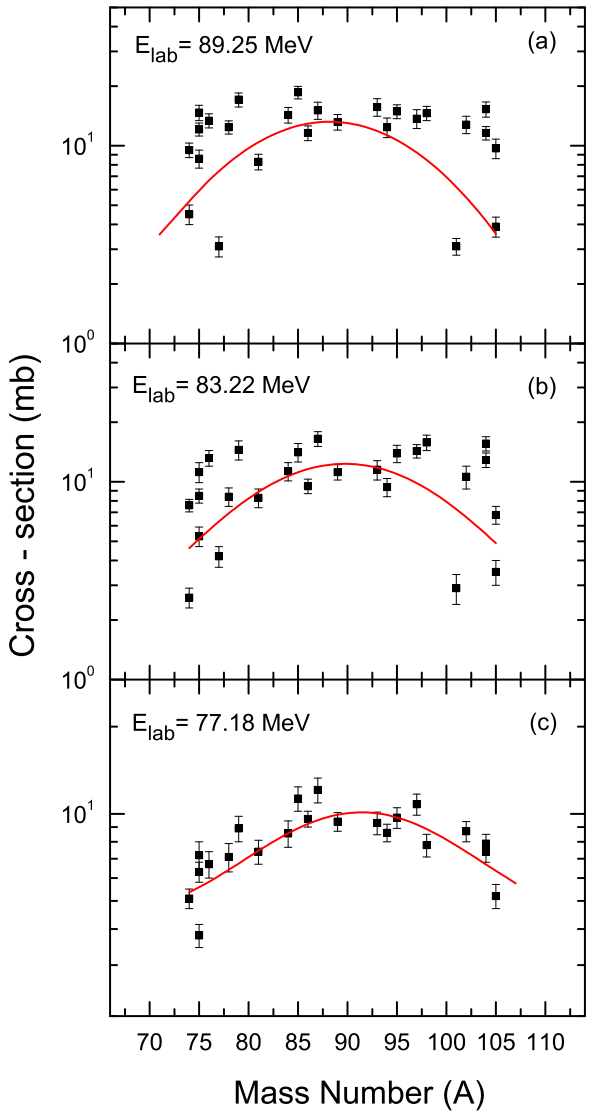

FIG. 3. Mass yields of fission products in $^{12}C + ^{169}Tm$ at E_{lab} = (a) 89.25 MeV, (b) 83.22 MeV, and (c) 77.18 MeV. The solid lines are the Gaussian fits through data points.

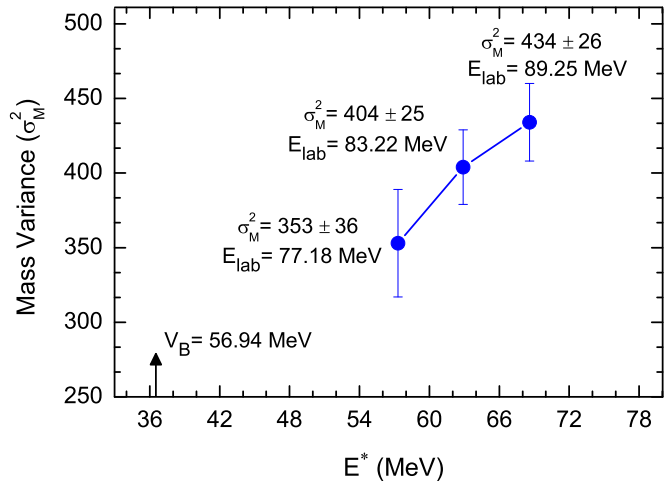

FIG. 4. Mass variance, σ_M^2, as a function of excitation energy (E^*) for a deformed thulium target. The solid lines show the increase in σ_M^2 with E^*. The arrow indicates the excitation energy corresponding to the Coulomb barrier.

leading to nuclear fission [24,44–46]. In heavy-ion induced reactions, the mass distribution of fission fragments is, generally, found to be symmetric because in most of the cases a compound nucleus is formed with an excitation energy which is well above the fission barrier. In order to obtain the mass distribution of fission fragments produced in $^{12}C + ^{169}Tm$ reactions at E_{lab} = 89.25, 83.22, and 77.18 MeV, experimentally measured cross sections of $^{74,75,76,77}Kr$, $^{101,102m,104,105}Tc$, $^{74m,75,84}Br$, ^{75}Ge, $^{86,93}Y$, $^{94,95}Ru$, ^{105}In, ^{81}Sr, $^{79,89}Rb$, $^{85,87}Zr$, ^{78}As, ^{104}Ag, and $^{97,98m}Nb$ residues are plotted as a function of mass number in Figs. 3(a)–3(c). The excitation energy and the maximum input angular momentum of the compound nucleus formed in the $^{12}C + ^{169}Tm$ reaction at incident projectile energies E_{lab} = 77.18, 83.22, and 89.25 MeV are estimated to be ≈57 MeV and ≈37$\hbar$, ≈63 MeV and ≈41$\hbar$, and ≈69 MeV and ≈45$\hbar$, respectively.

As shown in Figs. 3(a)–3(c), the mass distributions are found to be symmetric and can be fitted with one Gaussian function, indicating the formation of identified fission fragments from compound nuclear processes. The centroid and the width parameters, which represent most probable mass and dispersion of fission fragments, obtained from the analysis of mass distributions are found to be 88.18 ± 0.22 and 20.83 ± 0.62 at E_{lab} = 89.25 MeV [Fig. 3(a)], 89.76 ± 0.29 and 20.11 ± 0.63 at E_{lab} = 83.22 MeV [Fig. 3(b)], and 91.4 ± 0.5 and 18.80 ± 0.96 at E_{lab} = 77.18 MeV [Fig. 3(c)]. The variance of mass distribution σ_M^2 is found to be 434 ± 26 u^2 at E_{lab} = 89.25 MeV, 404 ± 25 u^2 at E_{lab} = 83.22 MeV, and 353 ± 36 u^2at E_{lab} = 77.18 MeV. The uncertainties quoted in these values are the fitting errors. In order to track the change in mass variance (σ_M^2) with excitation energy, the value of σ_M^2 obtained from the analysis of mass distributions of fission fragments at different excitation energies, E^* ≈ 69, 63, and 57 MeV, is plotted in Fig. 4.

The observed variation in the value of σ_M^2 with excitation energy for the present system follows the same trend as that reported by Ghosh *et al.* [9] for ^{19}F, ^{16}O, and ^{12}C projectiles on a deformed thorium, ^{232}Th, target. As shown in Fig. 4, the value of σ_M^2 increases with excitation energy, indicating larger spread in fission-fragment masses for higher excitation energies. The variation of the value of σ_M^2 with excitation energy at and below the barrier energies needs to be further investigated to better understand this aspect. In the present work, the variance of mass distribution agrees reasonably well with similar systems [24]. However, due to high angular momentum ($\langle l \rangle$ = 27.4$\hbar$) of the fissioning nucleus, variance of the mass distribution is larger than that of systems with the same fissility and at low angular momentum [13,47,48].

For better insights into the dynamics of fission, and to understand how distribution of fission fragments relates to the choice of entrance channel parameters, the mass variance of fission fragments for different projectile-target combinations has been plotted as a function of mass asymmetry,

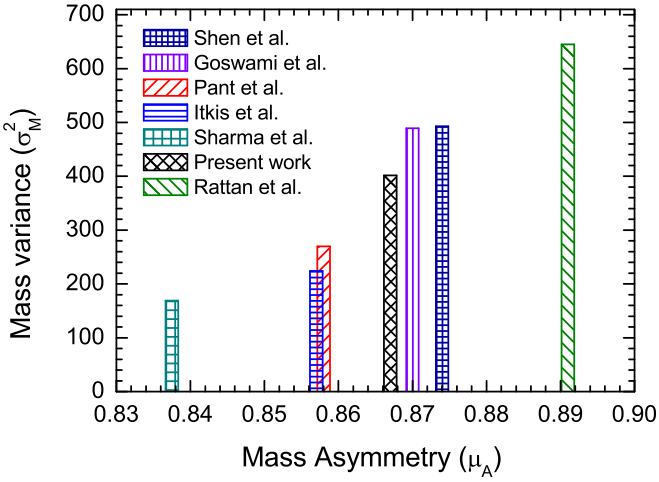

FIG. 5. Mass variance, σ_M^2, as a function of mass asymmetry, μ_A, of different projectile-target systems.

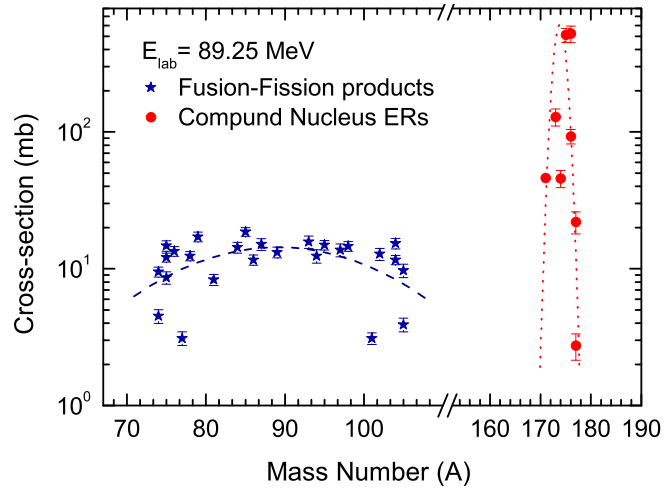

FIG. 6. Mass number vs cross sections for fission fragments and compound nucleus evaporation residues at $E_{\rm lab} = 89.25$ MeV populated in the $^{12}C + ^{169}Tm$ reaction. The dashed blue and dotted red lines through data points are drawn to guide the eyes.

$\mu_A = \frac{M_T - M_P}{M_T + M_P}$, in Fig. 5 [14,49–53]. As shown in this figure, the mass variance for the present system is consistent with the value reported by Sharma *et al.* [49] for the $^{16}O + ^{181}Ta$ system. The mass variance data presented in Fig. 5 for $^{16}O + ^{209}Bi$ [14], $^{16}O + ^{181}Ta$ [49], $^{238}U + ^{16}O$ [50], $^{16}O + ^{232}Th$ [51], $^{16}O + ^{208}Pb$ [52], and $^{12}C + ^{209}Bi$ [53] systems shows a linear increase in dispersion parameter (σ_M^2) with mass asymmetry (μ_A). This suggests broader distribution of fission fragments for more mass-asymmetric systems.

Further, the cross sections for all the evaporation residues identified in the present work at beam energy $E_{\rm lab} = 89.25$ MeV are plotted in Fig. 6 as a representative case. For heavy-ion induced reactions, the plot of mass number

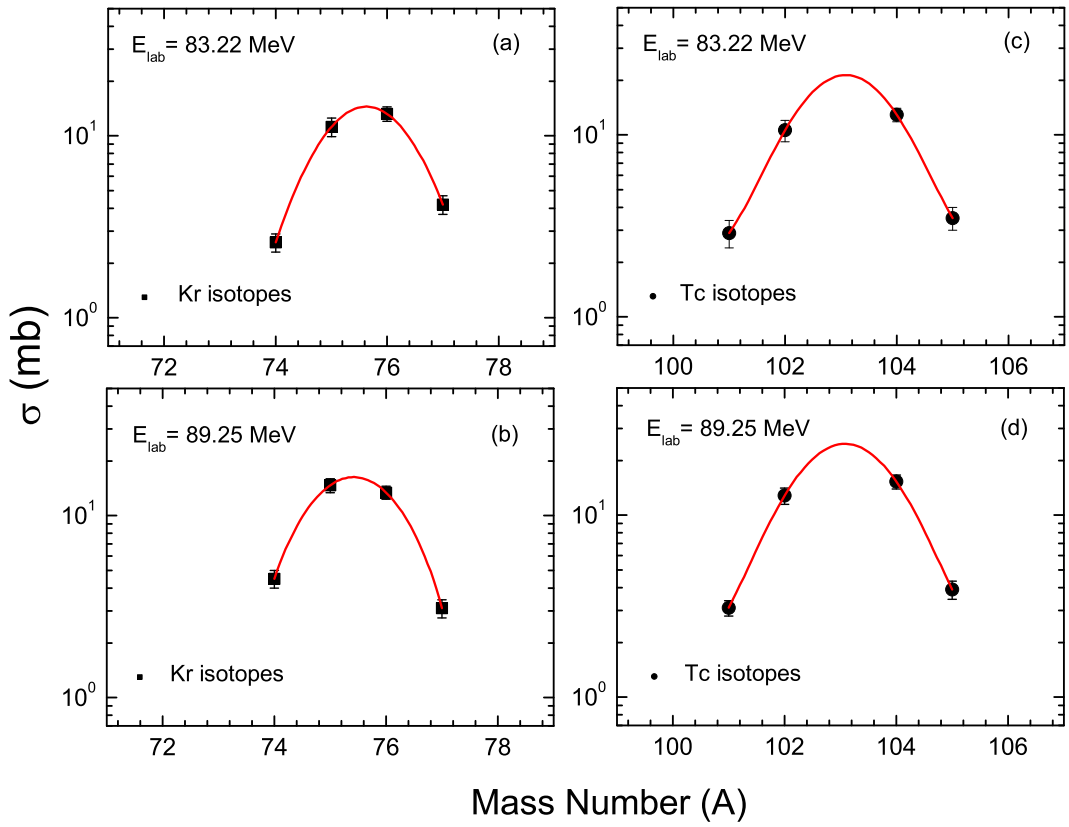

FIG. 7. Isotopic yield distribution of [(a) and (b)] krypton (^{74,75,76,77}Kr), and [(c) and (d)] technetium (^{101,102m,104,105}Tc) isotopes at $E_{\rm lab} = 83.22$ and 89.25 MeV. The solid lines show the fitted Gaussian distribution.

TABLE III. Charge distribution parameters for $E_{lab} = 89.25$ and 83.22 MeV in $^{12}C + ^{169}Tm$ system.

		89.25 MeV		83.22 MeV	
Isotope	Z	A_p	σ_A^2	A_p	σ_A^2
Kr	36	75.42 ± 0.03	3.90	75.63 ± 0.04	3.05
Tc	43	103.08 ± 0.04	3.27	103.1 ± 0.1	2.94

vs cross sections may have components from complete and/or incomplete fusion residues and fusion-fission residues. As is apparent from this figure, the wider peak at intermediate mass range corresponds to the fission-like events whereas the narrow peak at higher mass numbers is attributed to the complete and/or incomplete fusion events.

B. Isotopic yield distribution

At moderate excitation energies, neutron emission competes directly with the process of fission, as the emission of charged particle(s) is obstructed due to the large Coulomb barrier. Thus, nucleon emission from the primary fission fragments and/or fission of precursors of the fission-decay chains give rise to isotopic and isobaric yield distributions of the fission residues. To determine the total chain yield of a fission product with mass A and charge Z, values of the most-probable charge Z_p and the width parameter of charge distribution σ_Z for the isobaric mass chain are required.

In order to obtain these parameters, cross sections of at least three members in an isobaric chain should be measured. Since it is difficult to measure three independent yields in an isobaric chain, an alternative approach of isotopic yield distribution of the fission products was used to obtain the charge distribution parameters. In an isotopic chain, a fission product with mass A for fixed Z may result from subsequent evaporation of neutron(s) from several fragments.

Thus, its total yield $Y^{\text{total}}(A)$ may be related to the yields of the corresponding fragments $Y(A')$ using the relation

$$Y^{\text{total}}(A) = \sum_{\nu=1}^{n} P_\nu Y(A'), \tag{2}$$

where A' $(=A+\nu)$ is the mass number of the fragment emitting n neutrons to form the fission product with mass A, and P_n is the probability of emission of n neutrons by the fragment A'. The independent yields of the fission fragments are assumed to have a Gaussian charge distribution given by

$$Y(A') = \frac{Y_Z}{\sqrt{2\pi\sigma_{A'}^2}} e^{-(A'-A_p')^2/2\sigma_{A'}^2}, \tag{3}$$

where A_p' and $\sigma_{A'}^2$ are the most probable mass and variance of the isotopic yield distribution. Y_Z is the elemental yield. Substituting $Y(A')$ in Eq. (3) gives the total yield of the corresponding decay chain as

$$Y^{\text{total}}(A) = \sum_{\nu=1}^{n} P_\nu \frac{Y_Z}{\sqrt{2\pi\sigma_{A'}^2}} e^{-(A'-A_p')^2/2\sigma_{A'}^2}. \tag{4}$$

TABLE IV. Comparison of variance (σ_A^2) of isotopic yield distribution for different fissioning systems.

System	E^* (MeV)	Isotope	σ_A^2	Refs.
$^{12}C + ^{169}Tm$	68.6	Kr	3.90 ± 0.20	[a]
$^{12}C + ^{169}Tm$	68.6	Tc	3.27 ± 0.18	[a]
$^{12}C + ^{169}Tm$	62.9	Kr	3.05 ± 0.18	[a]
$^{12}C + ^{169}Tm$	62.9	Tc	2.94 ± 0.28	[a]
$^{16}O + ^{181}Ta$	67.04	Y	3.05 ± 0.10	[49]
$^{16}O + ^{181}Ta$	67.04	In	4.16 ± 0.01	[49]
$^{16}O + ^{159}Tb$	57.1	Sr	3.31	[54]
$^{16}O + ^{159}Tb$	57.1	Y	4.41	[54]
$^{16}O + ^{169}Tm$	61.06	In	4.24	[54]
$^{16}O + ^{169}Tm$	61.06	Tc	4.62	[54]
$^{7}Li + ^{232}Th$	41.7	Sb	4.08	[55]
$^{7}Li + ^{232}Th$	41.7	I	3.96	[55]
$^{11}B + ^{232}Th$	55.7	Sb	4.0	[22]
$^{11}B + ^{232}Th$	55.7	I	5.43	[22]
$^{11}B + ^{232}Th$	55.7	Cs	3.72	[22]
$^{11}B + ^{238}U$	67.4	Rb	3.84 ± 0.16	[56]
$^{11}B + ^{238}U$	67.4	Cs	3.95 ± 0.14	[56]
$^{22}Ne + ^{238}U$	64.5	Rb	4.23 ± 0.40	[56]
$^{22}Ne + ^{238}U$	64.5	Cs	4.26 ± 0.90	[56]
$^{20}Ne + ^{208}Pb$	46.4	Sb	3.43 ± 1.02	[57]
$^{20}Ne + ^{208}Pb$	46.4	I	3.95 ± 0.87	[57]

[a]This work.

The mean-squared deviation of the calculated isotopic yields $Y^{\text{total}}(A)$ from the respective experimentally determined yields $Y^{\text{exp}}(A)$ can be estimated by the χ^2 fit as given by

$$\chi^2 = \frac{1}{(m-p-1)} \sum_{j=1}^{m} \left[Y_j^{\text{total}}(A) - Y_j^{\text{exp}}(A)\right]^2. \tag{5}$$

The χ^2 minimization was done using a nonlinear least-square fit procedure, keeping width (σ_A) and most-probable mass (A_p') as the free parameters in Eq. (5). p is the number of free parameters, which is equal to 2 in the present case. Summation was carried over m isotopes of a given element. In the present work, the foregoing approach was used to obtain the charge distribution parameters from the experimentally measured independent yields of krypton (^{74,75,76,77}Kr) and technetium (^{101,102m,104,105}Tc) isotopes at energies 83.22 and 89.25 MeV. Mass dispersion curves and the corresponding parameters for Kr and Tc isotopes are obtained by fitting their respective independent yields to a Gaussian function. The fitted curves and the experimentally determined independent yields at both the energies are shown in Fig. 7. The values of most probable mass A_p for Kr and Tc isotopes at excitation energy $E^* \approx 69$ MeV corresponding to incident energy $E_{lab} = 89.25$ MeV are found to be 75.42 ± 0.03 and 103.08 ± 0.04, respectively. The width parameters σ_A for Kr and Tc isotopes are estimated to be 1.97 ± 0.07 and 1.81 ± 0.07, respectively. The uncertainties quoted for these parameters are the fitting errors. The measured charge distribution parameters evaluated from the analysis of isotopic yield distributions at energies $E_{lab} \approx 83.22$ and 89.25 MeV are presented in Table III. The isotopic yield distribution at $E_{lab} = 77.12$ MeV could not be

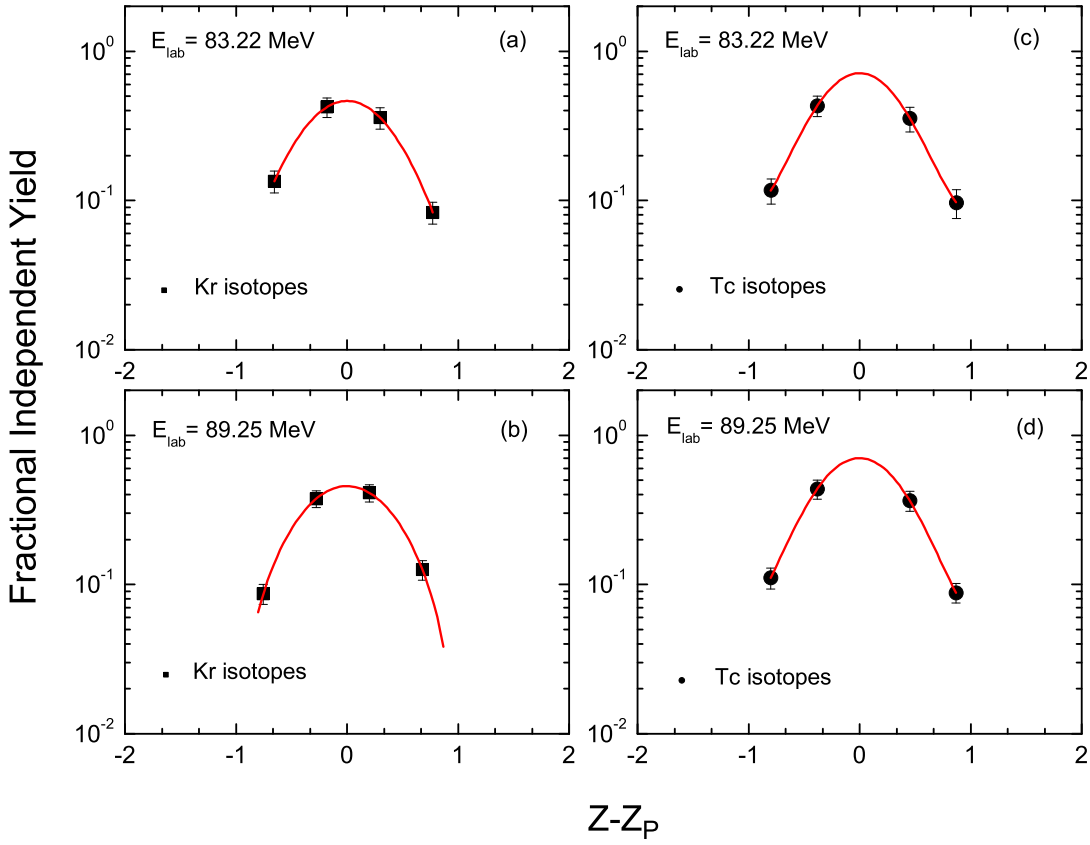

FIG. 8. Fractional independent yield distribution as a function of $Z - Z_p$ for [(a) and (b)] Kr isotopes at $E_{\rm lab} = 83.22$ and 89.25 MeV respectively. (c) and (d) are similar plots for Tc isotopes. The solid lines are the Gaussian fits to determine σ_z.

obtained, as the number of measured cross sections was not ample for distribution studies. The values of variance (σ_A^2) reported in the literature for a number of other fissioning systems at comparable excitation energies are presented in Table IV. It was found that the σ_A^2 values obtained in the present work for the ^{12}C + ^{169}Tm system are in the same range as the values for other systems presented in this table.

C. Isobaric yield distribution

Charge distribution studies gauge the distribution of nuclear charge between two complimentary fission fragments for a given mass division of the system undergoing fission. The charge distribution in nuclear fission is determined by (*i*) the most probable atomic number (Z_p) for the fission product which has the highest yield among all the products of given mass chain A, and (*ii*) the fractional independent yield for an isotope obtained by dividing the yield of the isotope by the total yield of the mass chain A to which it belongs. Based on the uncharged distribution (UCD) hypothesis [58], the most probable charge Z_p for Kr and Tc isotopes was obtained as

$$Z_p = \frac{A}{\frac{A_p}{Z}} \qquad (6)$$

Using Eq. (6), the value of $Z - Z_p$ was calculated for each isotope of Kr and Tc. The experimentally determined yields of Kr and Tc were normalized to obtain their respective fractional independent yields (FIY). Figure 8 shows the fractional independent yields of Kr and Tc as a function of $Z - Z_p$. The value of the isobaric charge dispersion parameter (σ_z) for Kr and Tc obtained from the fitting procedure is estimated to be 0.94 ± 0.05 and 0.75 ± 0.05 charge units, respectively. Further, the values of σ_z were calculated by converting the width parameter of isotopic yield (σ_A) to $\sigma_z = \sigma_A.Z/A_p$ as discussed in Ref. [59]. The value of σ_z calculated for Kr and Tc isotopes is found to be 0.942 and 0.754, respectively, which is in reasonably good agreement with the values obtained from the experimentally determined yields presented in Fig. 8. This indicates the self-consistency of the present analysis.

III. SUMMARY AND CONCLUSIONS

The production cross sections for various fission fragments were measured in the ^{12}C + ^{169}Tm system at energies $E_{\rm lab} =$ 77.81, 83.22, and 89.25 MeV. The mass distribution of fission fragments at different excitation energies was studied to probe dispersion of fission fragments. The mass dispersion of fission fragments was found to be symmetric at all the studied excitation energies, $E^* \approx 57$, 63, and 69 MeV, and can be fitted with one Gaussian function, indicating

the population of fission fragments via deexcitation of the compound nucleus. For better insights into the distribution of fission fragments, the dispersion of fission fragments σ_M^2 was studied in terms of excitation energy and mass asymmetry of interacting partners. It was found that the value of σ_M^2 increases with excitation energy and mass asymmetry, indicating broader distribution of fission fragments at larger excitation energies and for more mass-asymmetric systems. The isotopic and isobaric yield distributions of several fission fragments were studied to understand the dynamics of charge distribution. The charge distribution parameters were obtained from the analysis of experimental yields of Kr and Tc isotopes. It was found that the charge distribution parameters compare well with the experimental values reported in the literature.

ACKNOWLEDGMENTS

We thank the Director of IUAC New Delhi for providing all the necessary facilities to perform these experiments. P.P.S. thanks the Science and Engineering Research Board (SERB), India for Young Scientist Research Grant No. YSS/2014/000250, and S.A. acknowledges a research grant received from Aksaray University for Project No. 2016-053.

[1] O. Hahn and F. Strassmann, Naturwissenschaften **27**, 89 (1939).
[2] B. B. Back *et al.*, Phys. Rev. C **9**, 1924 (1974).
[3] C. Rubbia *et al.*, European Organization for Nuclear Research Report No. CERN/AT/95-44(ET), 1995 (unpublished).
[4] C. D. Bowman, Annu. Rev. Nucl. Part. Sci. **48**, 505 (1998).
[5] A. Baran, M. Kowal, P. G. Reinhard, L. M. Robledo, A. Staszczak, and M. Warda, Nucl. Phys. A **944**, 442 (2015).
[6] P. Moller and A. J. Sierk, Nature (London) **422**, 485 (2003).
[7] K. Nishio, H. Ikezoe, Y. Nagame, M. Asai, K. Tsukada, S. Mitsuoka, K. Tsuruta, K. Satou, C. J. Lin, and T. Ohsawa, Phys. Rev. Lett. **93**, 162701 (2004).
[8] D. J. Hinde, M. Dasgupta, J. R. Leigh, J. P. Lestone, J. C. Mein, C. R. Morton, J. O. Newton, and H. Timmers, Phys. Rev. Lett. **74**, 1295 (1995).
[9] T. K. Ghosh, S. Pal, K. S. Golda, and P. Bhattacharya, Phys. Lett. B **627**, 26 (2005).
[10] B. B. Back, H. Esbensen, C. L. Jiang, and K. E. Rehm, Rev. Mod. Phys. **86**, 317 (2014).
[11] W. J. Swaitecki, Phys. Scr. **24**, 113 (1981).
[12] C. Gregoire, C. Ngo, and B. Remaud, Phys. Lett. B **99**, 17 (1981).
[13] D. J. Hinde, D. Hilscher, H. Rossner, B. Gebauer, M. Lehmann, and M. Wilpert, Phys. Rev. C **45**, 1229 (1992).
[14] L. M. Pant *et al.*, Eur. Phys. J. A **11**, 47 (2001).
[15] T. Sikkeland *et al.* Phys. Lett. B **42**, 201 (1972).
[16] V. S. Ramamurthy and S. S. Kapoor, Phys. Rev. Lett. **54**, 178 (1985).
[17] J. V. Kratz, J. O. Liljenzin, A. E. Norris, and G. T. Seaborg, Phys. Rev. C **13**, 2347 (1976).
[18] D. J. Hinde, J. R. Leigh, J. J. M. Bokhorst, and J. O. Newton, Nucl. Phys. A **472**, 318 (1987).
[19] J. P. Lestone, J. R. Leigh, J. O. Newton, and J. X. Wei, Nucl. Phys. A **509**, 178 (1990).
[20] M. C. Duh, H. Baba, N. Takashi, A. Yokoyama, and T. Saito, Nucl. Phys. A **550**, 281 (1992).
[21] A. Pagano, S. Aiello, E. De Filippo, G. Lanzano, S. Lo Nigro, C. Milone, G. Blancato, G. Di Marco, and M. C. Mermaz, Phys. Rev. C **47**, 1170 (1993).
[22] G. K. Gubbi, A. Goswami, B. S. Tomar, B. John, A. Ramaswami, A. V. R. Reddy, P. P. Burte, and S. B. Manohar, Phys. Rev. C **53**, 796 (1996).
[23] N. Bohr and J. A. Wheeler, Phys. Rev. **56**, 426 (1939).
[24] S. B. Manohar, A. Goswami, and B. S. Tomar, J. Radioanal. Nucl. Chem. **203**, 331 (1996).
[25] Yu. Ts. Oganessian *et al.*, Nature (London) **400**, 242 (1999).
[26] V. M. Strutinsky, Nucl. Phys. A **95**, 420 (1967).
[27] P. Moller and S. G. Nilsson, Phys. Lett. B **31**, 283 (1970).
[28] P. Fong, Phys. Rev. **102**, 434 (1956).
[29] B. D. Wilkins, E. P. Steinberg, and R. R. Chasman, Phys. Rev. C **14**, 1832 (1976).
[30] Ch. Ngo, Prog. Part. Nucl. Phys. **16**, 139 (1985).
[31] G. K. Gubbi, A. Goswami, B. S. Tomar, A. Ramaswami, A. V. R. Reddy, P. P. Burte, S. B. Manohar, and B. John, Phys. Rev. C **59**, 3224 (1999).
[32] J. R. D. Todd, A. R. Wolf, J. J. Hogan, and D. J. Parker, J. Phys. G **19**, 187 (1993).
[33] V. S. Ramamurthy, S. S. Kapoor, R. K. Choudhury, A. Saxena, D. M. Nadkarni, A. K. Mohanty, B. K. Nayak, S. V. Sastry, S. Kailas, A. Chatterjee, P. Singh, and A. Navin, Phys. Rev. Lett. **65**, 25 (1990).
[34] FREEDOM: Data acquisition and analysis system designed to support the accelerator-based experiments at the Inter University Accelerator Centre, New Delhi, India (unpublished)
[35] U. Gupta, P. P. Singh, D. P. Singh, M. K. Sharma, A. Yadav, R. Kumar, B. P. Singh, and R. Prasad, Nucl. Phys. A **811**, 77 (2008).
[36] E. Brown and R. B. Firestone, *Table of Isotopes* (Wiley, New York, 1986).
[37] J. K. Tuli, *Nuclear Wallet Card*, National Nuclear Data Center (Brookhaven National Laboratory, Upton, NY, 2000).
[38] A. Gavron, Phys. Rev. C **21**, 230 (1980).
[39] R. Bass, Nucl. Phys. A **231**, 45 (1974).
[40] S. K. Kataria, V. S. Ramamurthy, and S. S. Kapoor, Phys. Rev. C **18**, 549 (1978).
[41] M. K. Sharma, P. P. Singh, D. P. Singh, A. Yadav, V. R. Sharma, I. Bala, R. Kumar, Unnati, B. P. Singh, and R. Prasad, Phys. Rev. C **91**, 014603 (2015).
[42] M. Blann, Phys. Rev. Lett. **27**, 337 (1971); NEA Data Bank Report No. PSR-146, Gif-sur-Yvette, France, 1991 (unpublished).
[43] S. Chakrabarty *et al.* Nucl. Phys. A **678**, 355 (2000).
[44] D. J. Hinde, A. C. Berriman, R. D. Butt, M. Dasgupta, I. I. Gontcher, C. R. Morton, A. Mukherjee, and J. O. Newton, J. Nucl. Radiochem. Sci. **3**, 31 (2002).
[45] M. G. Itkis, Yu. A. Muzychka, Yu. Ts. Oganessian, V. N. Okolovich, V. V. Pashkevich, A. Ya. Rusanov, V. S. Salamatin, G. N. Smirenkin, and G. G. Chubarian, Phys. At. Nucl. **58**, 2026 (1995).

[46] S. B. Manohar, A. Goswami, A. V. R. Reddy, B. S. Tomar, P. P. Burte, and S. Prakash, Radiochim. Acta **56**, 69 (1992).
[47] E. N. Gruzintsev, M. G. Itkis, V. N. Okolovich, and G. N. Smirenkin, Yad. Fiz. **40**, 616 (1984).
[48] Ye. N. Gruzintsev *et al.*, Z. Phys. A **323**, 307 (1986).
[49] V. R. Sharma, A. Yadav, P. P. Singh, M. K. Sharma, D. P. Singh, Unnati, R. Kumar, K. S. Golda, B. P. Singh, A. K. Sinha, and R. Prasad, Phys. Rev. C **84**, 014612 (2011).
[50] W. Q. Shen, J. Albinski, A. Gobbi, S. Gralla, K. D. Hildenbrand, N. Herrmann, J. Kuzminski, W. F. J. Müller, H. Stelzer, J. Tke, B. B. Back, S. Bjrnholm, and S. P. Srensen, Phys. Rev. C **36**, 115 (1987).
[51] A. Goswami, A. V. R. Reddy, B. S. Tomar, P. P. Burte, and S. B. Manohar, Radiochim. Acta **62**, 173 (1993).
[52] M. G. Itkis *et al.*, in *European Physical Society XV Nuclear Physics Divisional Conference on Low Energy Nuclear Dynamics*, edited by Yu. Ts. Oganessian (World Scientific, Singapore, 1995), p. 177.
[53] S. S. Rattan, A. Ramaswami, and S. B. Manohar, J. Radiol. Nucl. Chem. **242**, 551 (1991).
[54] P. P. Singh, B. P. Singh, B. Sharma, Unnati, M. K. Sharma, R. Prasad, R. Kumar, and H. D. Bhardwaj, Int. J. Mod. Phys. E **17**, 549 (2008).
[55] R. Tripathi, K. Sudarshan, S. Sodaye, B. S. Tomar, G. K. Gubbi, A. Goswami, A. V. R. Reddy, and S. B. Manohar, Radiochim. Acta **90**, 185 (2002).
[56] M. de Saint-Simon *et al.*, Phys. Rev. C **14**, 2185 (1976).
[57] R. Tripathi, K. Sudarshan, A. Goswami, P. K. Pujari, B. S. Tomar, and S. B. Manohar, Phys. Rev. C **69**, 024613 (2004).
[58] W. Reisdorf, M. de Saint-Simon, L. Remsberg, L. Lessard, C. Thibault, E. Roeckl, and R. Klapisch, Phys. Rev. C **14**, 2189 (1976).
[59] H. Freiesleben and J. V. Kratz, Phys. Rep. **106**, 1 (1984).